J. Nanoanalysis., 6(3): 145-156, Summer 2019

ORIGINAL RESEARCH PAPER

Preparation and characterization of fluorapatite-bioactive glass S53P4 nanocomposite

Sahebali Manafi [1,*], Fatemeh Mirjalili [2], Mahmood Hajisafari [3], Faranak Orand [3]

[1] Department of Engineering, Shahrood Branch, Islamic Azad University, Shahrood, Iran
[2] Department of Material Engineering, Maybod Branch, Islamic Azad University, Maybod, Iran
[3] Department of Material Engineering, Yazd Branch, Islamic Azad University, Yazd, Iran

Received: 2019-02-03 Accepted: 2019-05-30 Published: 2019-06-20

ABSTRACT

This research has been done to study characteristic and biocompatible evaluation of a nano-biocomposite ceramic with the bioglass (BG) as a first phase. In this regard, synthesis of S53P4 (53% SiO_2, 4% P_2O_5, 23% Na_2O and 20% CaO) bioglass has been considered as the first phase and flourapatite (FA) considered as the second phase. Afterwards, nanocomposite with the base of S53P4 bioglass has been synthesized by sol-gel method. The synthesized nanoparticles and nanocomposite have been characterized with the help of different techniques, using field emission scanning electron microscope (FESEM), X-ray diffraction (XRD), Fourier transforms infrared spectroscopy (FT-IR), X-ray fluorescence (XRF) to evaluate crystal structure, microstructure, and morphology. The results showed that the crystallite size and the crystallinity of S53P4 bioglass-fluorapatite nanocomposites were about 20-30 nm and 70-90%, respectively. The FT-IR analyses displayed that the purity in the structure of this nanocomposite. The result of MTT (3-(4,5-Dimethylthiazol-2-Yl)-2,5-Diphenyltetrazolium Bromide) assay indicated the nontoxicity and also decreasing of cell viability in 7 days compared with the first day.

Keywords: *Biocompatible, Bioglass, Fluorapatite, MTT Assay, S53P4*

How to cite this article
*Manafi S, Mirjalili F, Hajisafari M, Orand F. Preparation and characterization of fluorapatite-bioactive glass S53P4 nanocomposite. J. Nanoanalysis., 2019; 6(3): 145-156. DOI: 10.22034/jna.****

INTRODUCTION

Bacterial infection is a severe problem consequent to implant surgery in orthopedics and dentistry, which can classically only be cured by removing the implant, since the biofilm mode of growing of infecting organisms on an implant surface defends the bacteria from the host immune system and antibiotic therapy [1]. Orthopedic implant infection control due to the use of antibiotics in long-term period, the surgery duplication rate, and clinical and economic outcomes is difficult to apply [2-3]. Nowadays, the use of biocompatible synthetic materials to exchange damaged tissues is considered as an essential and unavoidable condition [4]. Bioceramics is essential divisions of biomaterials, which are employed in a variety of clinical applications, counting dental materials, spinal cord repair, orthopedic applications, and drug delivery in the form of powder, coating, and bulk [5-7].

Of the bioactive materials, the best bioactive performance belongs to hydroxyapatite (HA) and bioactive glass (BG) bioceramics [8-10]. The combination of BG particles with HA makes special characteristics such as bioactivity and mechanical properties [11-13]. It was understood well that the insertion of fluoride ions in the HA structure significantly increases its resistance against biodegradability and thermal decomposition [14-17]. If OH^- groups in HA are completely replaced with F^-, fluorapatite (FA) is formed [11,18]. Microorganisms have a strong tendency

* Corresponding Author Email: *ali_manafi2005@yahoo.com*

to cause surfaces to form a micro-ecosystem in which various microbial strains and species grow in a slime-enclosed biofilm [3,19,20]. This ion replacement has a positive impact on proliferation, morphology and differentiation of osteoblast-like cells and improves bioactivity [13, 21,22].

Researchers found that adding of fluoride ions into hydroxyapatite structure increases its resistance to biodegradability meaningfully. Furthermore, by better absorption of protein, expresses a stronger cellular connection and reinforces the activity of phosphates that produce stronger osteoconductivity [13,23]. There are 1 worth. % fluorine (10,000 parts per million) in the cortical bone. The presence of this level of fluorine in the bone stops loss of bone density, which is the aim of osteoporosis [16,24]. Flourapatite also forms the outer layer of tooth [18]. The mineral phase of tooth under the enamel covers about 0.04-0.07 wt.% fluorine [19,25]. The enamel contains of flourapatite with the substitution of 50% F^- with OH^- [20,26]. S53P4 bioglass is a distinguished biomaterial due to its single set of properties such as unmatchable biocompatibility, outstanding bioactive manners and antibacterial characteristics [27-30]. BG the first reported bioactive glass, was produced by Professor Larry Hench in 1969 with a composition of 45 wt.% SiO_2, 24.5 wt.% Na_2O, 24.5 wt.% CaO and 6 wt.% P_2O_5 [4,31]. This discovery was also the beginning of second generation biomaterials that have the capability to bond with host tissues [4,32]. The most astounding feature about the BG finding was its ability to develop very strong interfacial bonds with surrounding tissues.

Moreover, BG has the highest *in vivo* bioactivity index (IB>8) among all bioceramicsc [6,33]. In spite of its astounding biocompatibility and bone bonding capability, BG has limited demands as a scaffold material due to its poor mechanical properties [7,34]. The combination of bioactive glass particles with flourapatite affords its special properties such as augmentation of bioactivity and mechanical properties. The novelty of this study is a combination of fluorapatite with S53P4 bioglass in order to produce fluorapatite/S53P4 bioglass compares its properties with hydroxyapatite/ bioactive glass. The present study aims to synthesize and characterize fluorapatite, bioactive glass and fluorapatite/bioactive glass nanocomposite by sol-gel method for bone tissue and evaluating their bioactivity using *in vitro* method. The target of this project is to develop and evaluate a ceramic glass nanosized composite with properties close to bone properties and good biocompatibility for use in dentistry and orthopedics as a bone constructor.

Preparation of S53P4 bioactive glass

At first, hydrolysis of 22.48 ml of tetraethoxysilane (TEOS) in 350 ml of distilled water and 350 ml of ethanol at room temperature and then, adjusted of pH at 2 by nitric acid with continuous stirring for 1 h. Then, the addition of 8.97 g of calcium nitrate hydrate to the above solution and continues stirring until dissolving. After that, the addition of 1.55 g of $NaNO_3$ to the above mixture (the previous mixture was named solution A) and then, 3.34 g of ammonium dehydrogenase phosphate was added to the distilled water (this mixture was named solution B). Furthermore, solution (B) was gradually added on solution (A) with continuous stirring for overnight. The resulted sol was filtrated and washed with distillate water for 3 times and with ethanol for 1 time using centrifuge with 1650 rpm for 10 min. Drying of the washed gel at 70 °C for overnight and sintered at 620 °C for 2 h.

Preparation of flourapatite powder

First, 11.82 g hydrated calcium nitrate ($Ca(NO_3).4H_2O$) was dissolved in 30 ml absolute ethanol/water, and also, another solution was made by dissolving 2.13 diammonium hydrogen phosphate [$(NH_4)_2HPO_4$] in 30 ml ethanol/distilled water. Both solutions were stirred to obtain transparency for 1 h. In the second step, the aqueous solution was added drop wise at a rate of 5 ml/min to alcoholic solution with vigorous stirring. The pH of the solution was regulated in 10 by drop wise addition of NH_4OH solution. In order to synthesize flourapatite (FA), to the solution of hydrated calcium nitrate and di-ammunium hydrogen phosphate, a solution of 0.56 g ammonium fluoride (NH_4F) with 30 ml ethanol/water was added. A milky and gelatinous precipitate was obtained. The obtained precipitates were centrifuged and washed by ethanol four times, dried at 80 °C for 5 h, and subsequently grinded with mortar and pestle. Finally, the resulting fine FA powders were heated to 600 °C for 1 h.

Preparation of FA/BG Nanocomposite

For synthesis of bioactive glasses of S53P4-fluorapatite nanocomposites with 10, 20 and 30% wt.% of bioactive glasses, two sols of bioactive glass and fluorapatite which mentioned were prepared.

Then, two sols were combined and stirred for 2 h using a magnetic stirrer. The obtained sol was maintained at ambient temperature with a different weight ratio for 14 days until it became uniform and transparent gel. The obtained precipitates were centrifuged and washed by ethanol four times, dried at 80 ºC for 5 h, and subsequently grinded with mortar and pestle. Finally, the resulting fine nanocomposite powders were heated to 600 °C for 1 h.

Characterization of and FA/BG Nanocomposite

Phase identification was performed by X-ray diffraction (XRD) PW1800, of Philips Company, using nickel filtered Cu-K_{α} radiation in the range of 2θ=20°-70° with a scanning speed of 5° per minute. A Fourier transform infrared spectrometer (FT-IR) by Perkin Elmer Spectrum 100 series was used by the universal attenuated total reflection (UATR) method. Microstructures of powders were identified by transmission electron microscope (Philips–Zeiss-Germany) and scanning electron microscopy (SEM PHENOM) and field emission scanning electron microscope (FESEM). Test samples were loaded at a testing machine (Instron 5569, Instron corp., Canton, U.S.) to measure the compressive strength at a crosshead speed of 1 mm/min.

To study and evaluate the thermal behavior of a S53P4 glass powder and to estimate the calcination temperature as well as the crystallinity and the simulated particle size of 45S5 bioglass, the simultaneous thermal analysis (STA,) NETZSCH STA 449 F1, Germany) was performed.

Evaluation of cell survival by MTT test

In the next step, the proliferation and survival of L929 cells on the surface of the samples were evaluated by MTT (3-(4,5-Dimethylthiazol-2-Yl)-2,5-Diphenyltetrazolium Bromide) assay. To prepare the samples, a common protocol for this test was used. In this way, 5 mg of each of the samples was mixed in the medium and incubated at 37 °C for 72 h. These samples were filtered to prevent contamination. After extracting the cells desired in the culture plate, the number of wells was considered as controls and some were considered as the test samples. After the desired time, the culture medium was discarded and a certain volume of solution was spilled on the cells and then, the cells were incubated in this solution. At this time, the MTT ring was broken, breaking the ring created crystalline purplish color. The amount of this color was directly related to the living cells. Next, the supernatant was discarded and the cells were washed. At the end, the absorbance of the solution was calculated by the spectrophotometer. The following formula is then used to determine the survival rate (1 equation):

$$\text{Cell Viability\%} = \frac{ODs}{ODc} \quad (1)$$

ODs Optical Density Sample, ODc Optical Density Control.

CHARACTERIZATION OF MATERIALS

X-ray diffraction analysis on the bioactive glass

Fig. 1 shows the XRD patterns of the S53P4 bioactive glass. Based on the X-ray diffraction pattern, it was represented a broader, shorter form that expressed the amorphous structure of the nanopowder synthesized. Although, the high degree of amorphous was detectable from this pattern, the peaks belonging to the crystalline

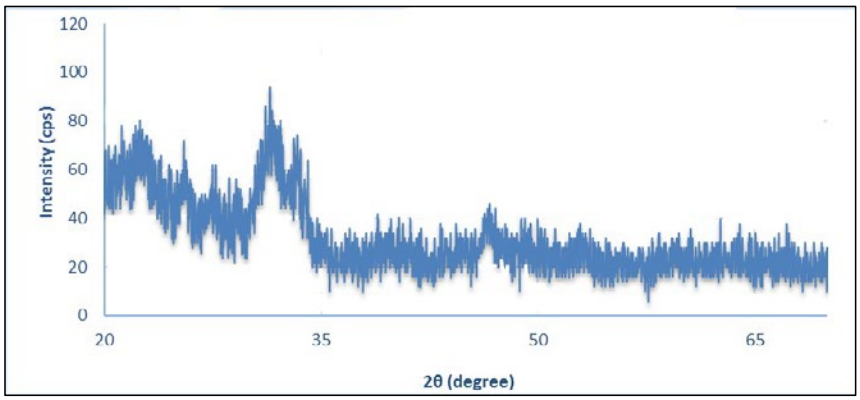

Fig. 1. X-ray diffraction pattern of synthesis of S53P4 bioglass nanopowder

phases were visible at angles 2θ=33 and 42 °C that was related to the effects of crystalline phases of calcium silicate $CaSiO_3$ or wollastonite (JCPDS 42-0547) and the peaks belonging to the crystalline phases were visible at angles 2θ=22 and 48 °C that was related to the effects of crystalline phases of sodium calcium silicate $Na_2CaSi_2O_6$ (JCPDS 77-2189) with anatomical crystalline structure.

Fig. 2 shows the X-ray diffraction pattern of the fluorapatite sample. It was known that all the peaks identified in the diffraction pattern were related to the structure of fluorapatite (JCPDS No. 00-003-0736) with a hexagonal crystal structure. In the interpretation of the diffraction pattern, it could be presented that, this structure was well crystal lined.

Finally, in this template, there were no peak spells belonging to other phases indicating the purity of the powder. The average crystallite size for synthesized fluorapatite nanoparticles was obtained at about 26 nm. The crystallinity (% Xc) in the synthesized fluorapatite nanoparticles was obtained at about 99%.

Figs. 3-5 show the X-ray diffraction pattern of the fluorapatite/S53P4 bioglass composite samples. The synthetic nanosized particles were distinguishable from the synthesized composite dispersion pattern. The presence of glass in the material structure has led to the expansion of the diffraction pattern of the materials. By examining the patterns, it can be said that, because of the overlapping of the amorphous peak of the glass phase with apatite peaks in the range of 2θ=25 to 35 degrees, the amorphous peak of the glass was not very distinct and only led to the shift or displacement of the apatite characteristic peaks. Adding the glass phase to fluorapatite would lead to gradual spreading of diffraction peaks, which would also affect the reduction of crystallinity and reduce the size of the crystal based on the data (XRD) as shown in Table 1.

Simultaneous thermal analysis (STA) of S53P4 bioglass

The results of the TG/DTA test performed on a S53P4 dry gel (before stabilization or calcination)

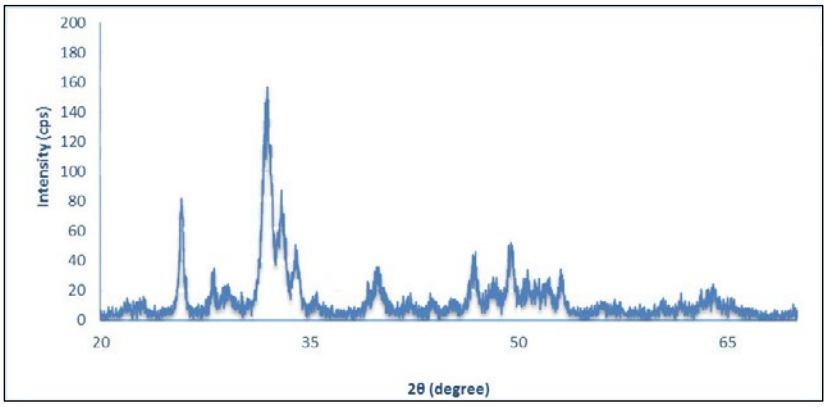

Fig. 2. X-ray diffraction pattern of fluorapatite nanoscale

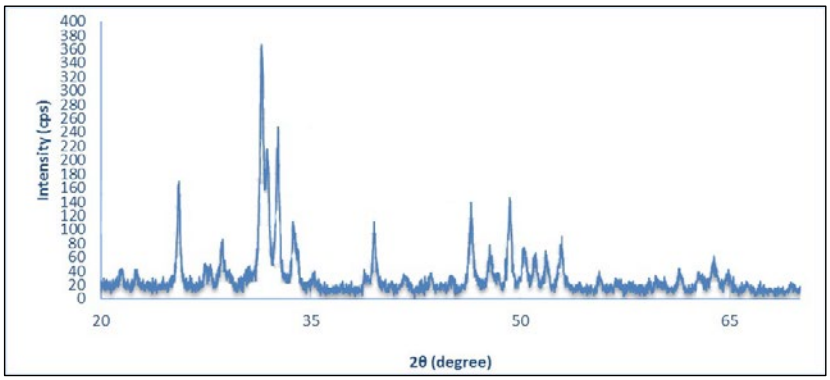

Fig. 3. X-ray diffraction pattern of 10% S53P4 BG-FA nanocomposite

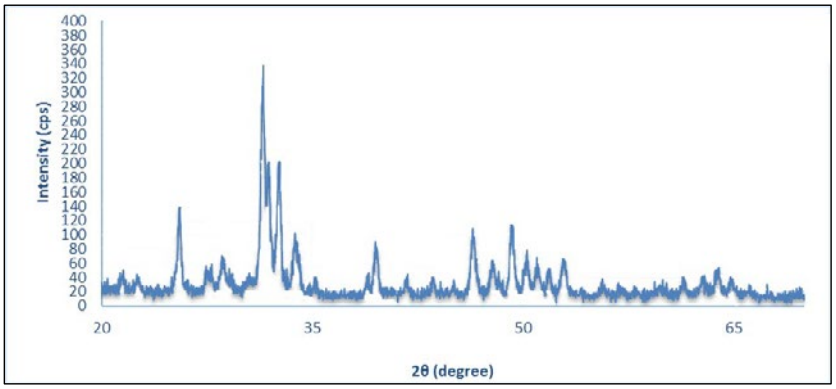

Fig. 4. X-ray diffraction pattern of 20% S53P4 BG-FA nanocomposite

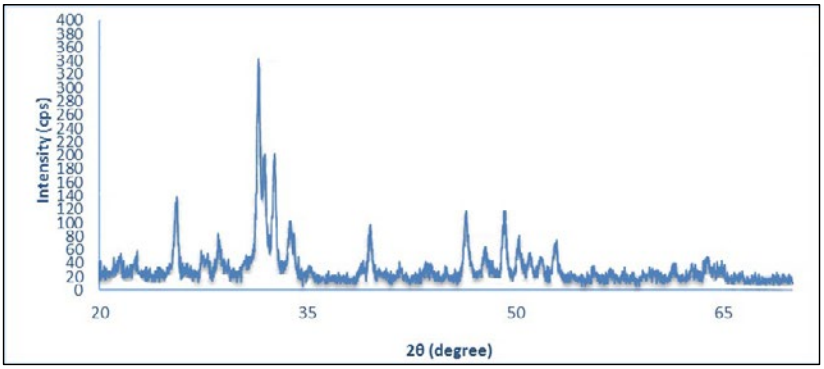

Fig. 5. X-ray diffraction pattern of 30% S53P4 BG-FA nanocomposite

Table 1. Comparison of particle size and crystallite percentage of composites

Sample	Particle size	Crystallite percentage
10% S53P4	28 nm	86%
20% S53P4	24 nm	71%
30% S53P4	20 nm	67%

Table 2. The weight loss of gel with temperature increasing

Weight loss			Sample
Stage 3 750-1000 °C	Stage 2 200-660 °C	Stage 1 25-190 °C	
2%	37%	1%	BG-100%

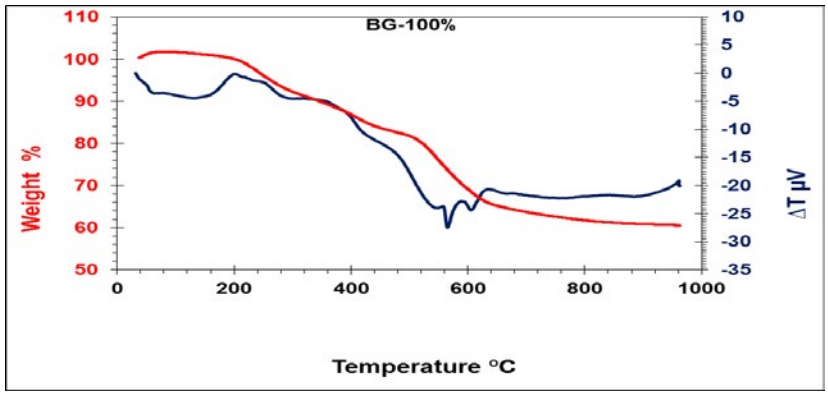

Fig. 6. STA analysis of S53P4 bioglass

in the range of 25-1000 °C indicated a few incidences (Fig. 6). In the temperature range of 25-190 °C, an endothermic reaction occurred which related to the exit of moisture and the

liquids in the dry gel. At temperatures of 190-640 °C, several endothermic and exothermic reactions were attributed to the degradation of organic elements such as silanol groups or the onset of nitrate decomposition reactions. The thermal decomposition of nitrates was a phase reaction that occurred thermodynamically at temperatures below 550 °C.The major part of organic detoxification and subsequent weight loss occurred at a temperature of 540-640 °C. With regard to the TGA curve, after the thermal decomposition of the nitrates, the mass changes in the specimens became constant and stable. Then, an exothermic peak was observed at temperature of about 750 °C which can be attributed to the crystallization process of the glass. The weight variation curve with temperature can be divided into three regions which was shown in Table 2.

One of the steps to be taken into account in the bioactive action of bioactive glasses was the formation of Si-OH groups of surface that were actually apatite germination sites. Also, the sol-gel synthesized glass inherently contained hydroxyl groups in their own network. On the other hand, the specific surface area and the amount of hydroxyl groups decreased by increasing of the temperature and the crystallization increased. Therefore, the reduction of the bioactivity of the bioglass occurred. At around 640 °C, almost all nitrates were removed from the glass network. Therefore, the temperature of 650 °C was chosen as the appropriate stabilization temperature for the biologically active glass. The selection of high temperatures led to crystallization in glass and thus the production of ceramic glass.

The results of X-ray fluorescence spectroscopy

In order to confirm the existence of the elements of the S53P4 bio accumulated glass in the sample, the chemical analysis results from the pure bioactive glass sample was prepared in Table 3. Based on these results, it could be seen that, the analysis of synthesized S53P4 nanopowder was very close to the standard glass of S53P4 and the difference in percentage by weight could be attributed to the presence of impurities.

FT-IR analysis of S53P4 bioglass

Fig. 7 shows Infrared spectroscopy analysis of S53P4 bioglass. The graph shows seven obvious bands, the first band at 464 and 803 cm^{-1} which was characteristic to Si–O–Si bending and the second band at 510 cm^{-1} was correlated to phosphate group (PO_4^{3-}).

The band at 1100 cm^{-1} was related to (PO) and at 966 cm^{-1}, the band characterized to SiO_2 stretching band. The last band at 3452 cm^{-1} was collocated to O-H. Fig. 8 shows the FT-IR spectrum of the synthesized fluorapatite nanoparticles. The relevant FT-IR spectrum had all vibrations v_4 to v_1 related to the phosphate group in the structure of apatite. Finally, there were the two courier sharps of 564 cm^{-1} and 603 cm^{-1} belonging to the group of v_4 vibrations. The presented peak at 741 cm^{-1}

Table 3. The XRF analysis of the Standard S53P4 glass and synthesized S53P4 bioglass

Materials	SiO_2 wt.%	Na_2O wt.%	CaO wt.%	P_2O_5 wt.%
Standard glass of S53P4	53.0	23.0	20.0	4.0
Synthesized glass of S53P4	53.52	21.47	20.63	4.38

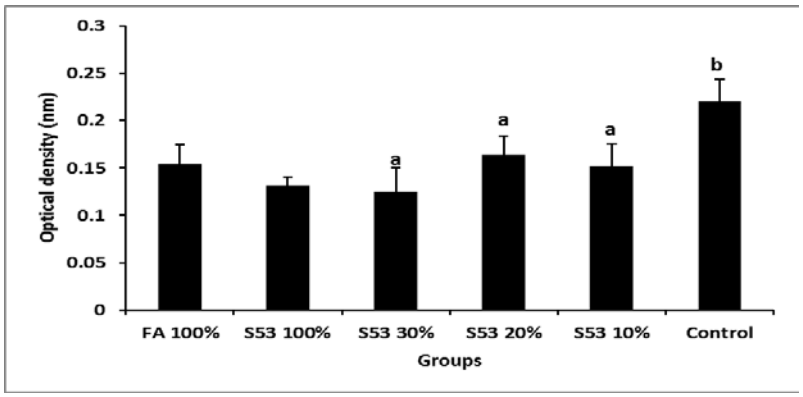

Fig. 7. Infrared spectroscopy analysis of S53P4 bioglass

represented the hydroxyl chain, which was found in this structure that is rich of fluorine. The peaks at wave numbers of 1640 cm^{-1}, 3700 cm^{-1} were related to O-H groups. A central peak of 873 cm^{-1}, along with a band with two edges of 1413 cm^{-1} and 1465 cm^{-1} was attributed to structural carbonate CO_3^{2-} groups. The presence of this group represented the bioavailability of fluorapatite.

Structural changes at fluorapatite-S53P4 bioglass nanocomposite samples with different S53P4 bioglass percentages were investigated by FT-IR, which could be observed in Figs. 9 (A-C). The peak at wave numbers of 923 cm^{-1} was related to v_1 vibration and the peak at wave number of 464 cm^{-1} was related to v_2 vibration and the wide peak at wave numbers of 1047 cm^{-1} was related to v_1 vibration which was the tensile vibration of the tetrahedral phosphate (PO_4^{3-}) group. Finally, two sharp peaks were located at 567 cm^{-1} and 607 cm^{-1}, which were belong to the v_4 vibration of PO_4^{3-} group. Additionally, with increasing the percentage of fluorapatite phase, a strong and broad absorption band of the glass phase in the wavelength range of 1200-100 cm^{-1} which was related to the tensile vibrations of the Si-O-Si and P-O groups are gradually narrowed and focused to 1047 cm^{-1}.

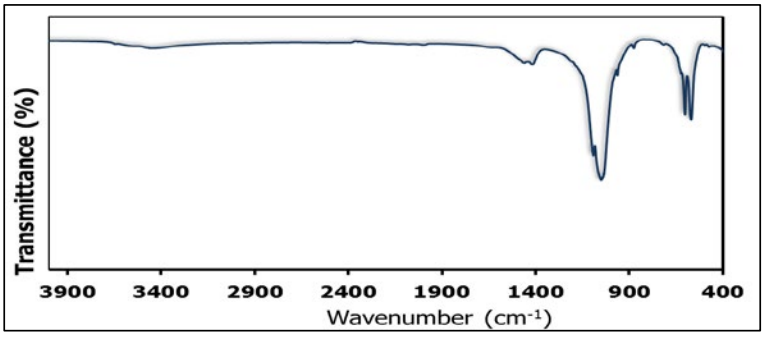

Fig. 8. FT-IR analysis of bioactive fluorapatite

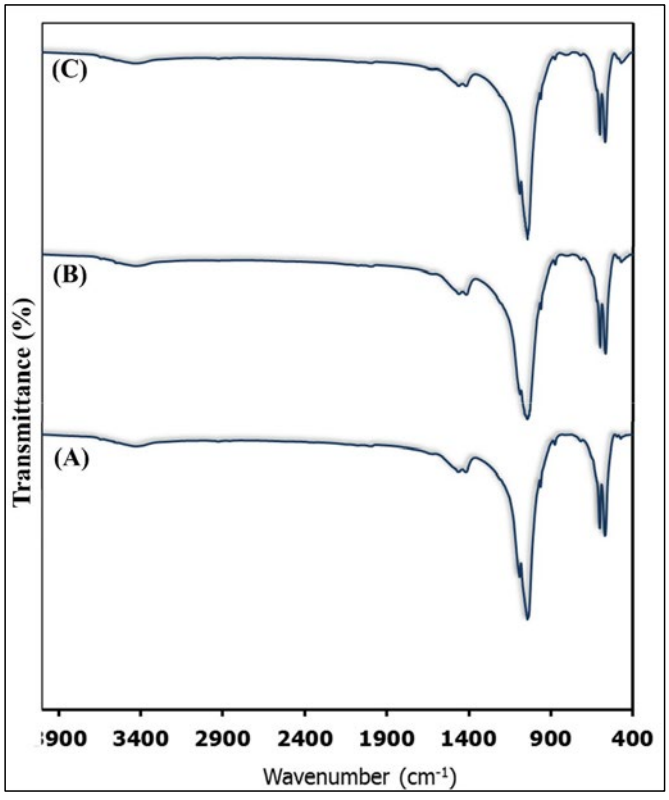

Fig. 9. Infrared spectroscopy analysis of FA-S53P4 BG nanocomposite, A) 10%, B) 20%, C) 30%.

Raman spectroscopy analysis of S53P4 bioglass

The Raman spectrum of the synthesized S53P4 bioglass sample in the wavelength range of 800-1200 cm^{-1} was based on a very broad-edge courier with two concentrated absorption edges of 995 cm^{-1} and 1115 cm^{-1}, respectively, to the symmetric tensile vibrations of the phosphate group $PO4^{3-}$) and asymmetric tensile vibrations of poly-oxygen in the Si-O-P group (Fig. 10). The broad and non-distinct nature of the peaks can be attested to the amorphous structure of the synthesized sample.

The Raman spectrum in the spectral range of 100-1200 cm^{-1} of flourapatite in Fig. 11 shows the results as follows: Peak at 965 cm^{-1} was attributed to the symmetrical tensile vibrations of the phosphate group, which indicated the structure of the fluorapatite. Several low intensity peaks at 1030-1050 cm^{-1} were associated with the asymmetric tensile vibrations of the phosphate group. Peak at 1081 cm^{-1}refered to the vibrations of the carbonate group in the fluorapatite.

The Raman spectrum of S53P4 bioglass-fluorapatite nanocomposite samples with different S53P4 bioglass percentages were shown in Figs. 12 (A-C). In all samples peak at 1081 cm^{-1} referred to the vibrations of the carbonate group in the fluorapatite. Another peak appeared in the samples, which was at 1080 cm^{-1}, which was in the structure of carbonates. And the peaks were appeared at 1115 cm^{-1} related to the Si-O-P group.

Morphological properties of nanopowders and nanocomposites by FESEM

Fig. 13a illustrated the FESEM images of synthesized S53P4 particles. It can be clearly demonstrated that, the nanoparticle had spherical morphology with some agglomeration, which was due to the intrinsic nature of nanoparticles and their particle size ranges was from 40 to 25 nm. A FESEM microsphere of the synthesized fluorapatite nanoparticles was shown in Fig. 13b.

It was indicated the formation of nanometric particles with spherical morphology and a particle size range of 20-35 nm.

The proposed EDS (Energy Dispersive X-Ray Spectroscopy) pattern for synthesized S53P4

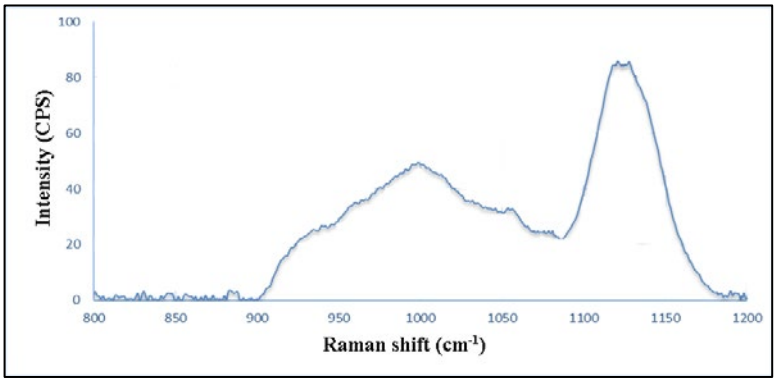

Fig. 10. S53P4 bioglass spectroscopy test

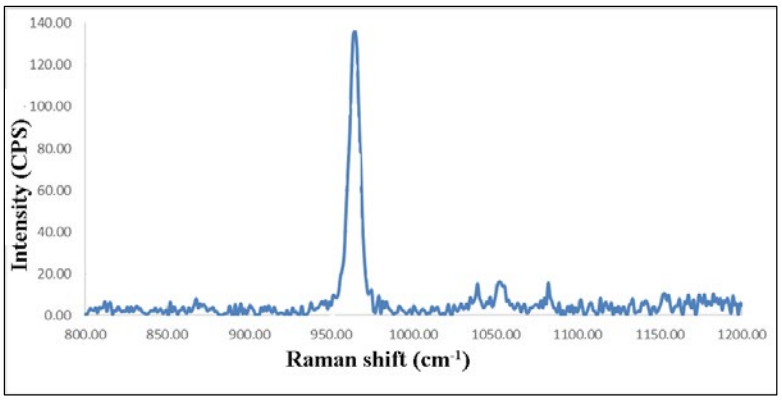

Fig. 11. Flourapatite spectroscopy test

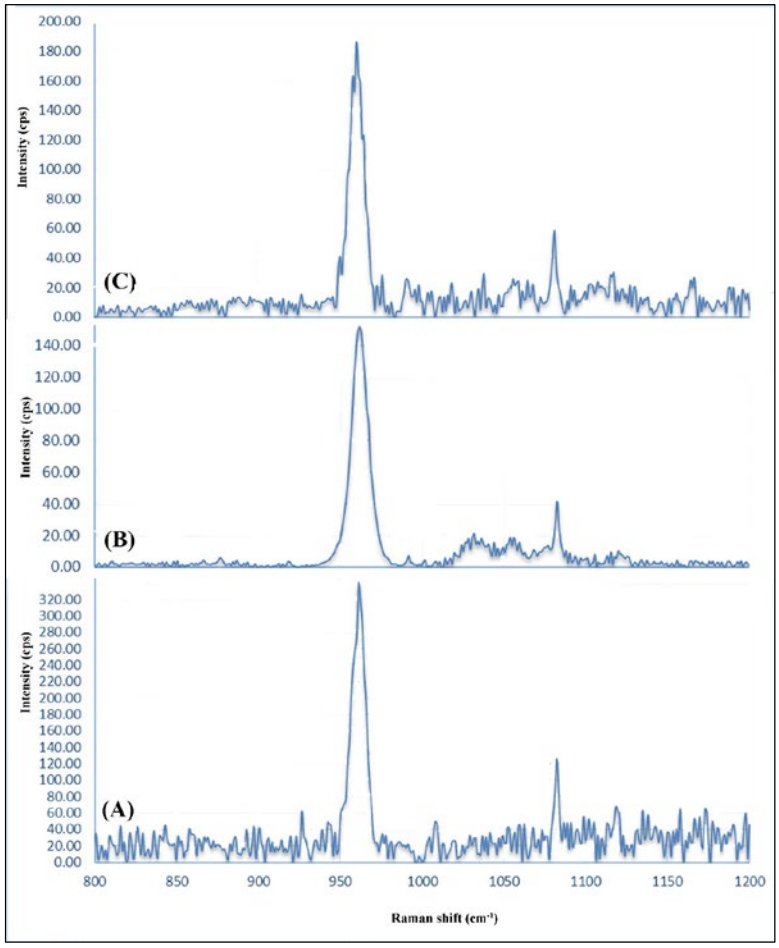

Fig. 12. Spectrophotometric test of FA- S53P4 BG nanocomposite, A) 10%, B) 20%, C) 30%.

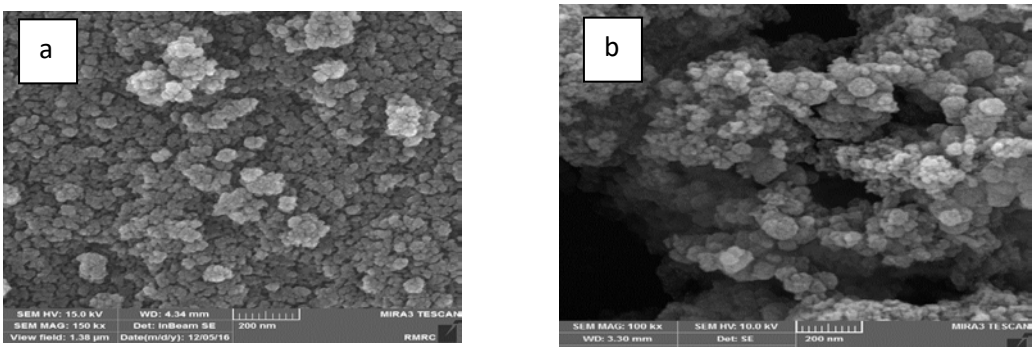

Fig. 13. Field emission SEM images of a) S53P4 bioglass, b) fluorapatite nanopowders

biologically active glass in Fig. 14(a) indicated the appearance of peaks related to the main elements of the glass constituent, namely, silicon, calcium, sodium, phosphorus and oxygen. In the EDS pattern of the fluorapatite in Fig. 14(b), there were four main elements consisted of calcium, phosphorus, fluorine and oxygen. Field emission scanning images of S53P4 bioactive glass-fluorapatite nanocomposites with different percentages of S53P4 bioglass was shown in Fig. 15a-c. As it was shown the spherical shape of these synthesized particles with different particle size in three samples from about 20 nm to 40 nm, which confirmed the XRD results.

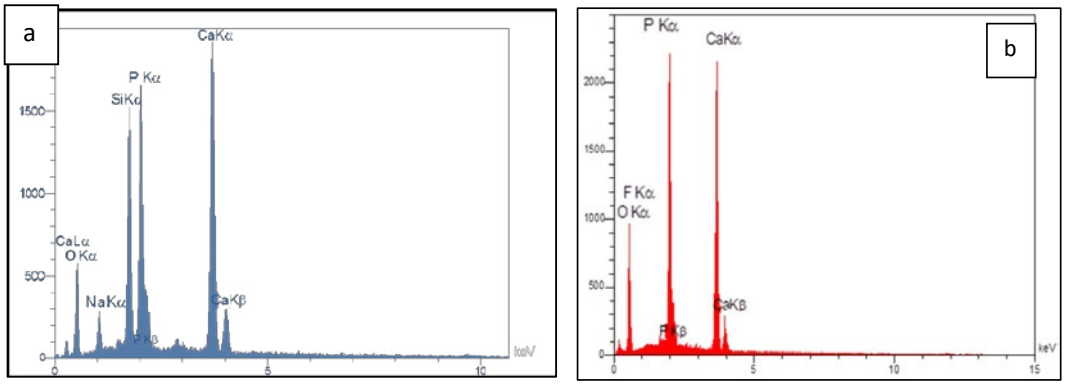

Fig. 14. EDS Analysis of a) S53P4 bioglass, b) fluorapatite nanopowders

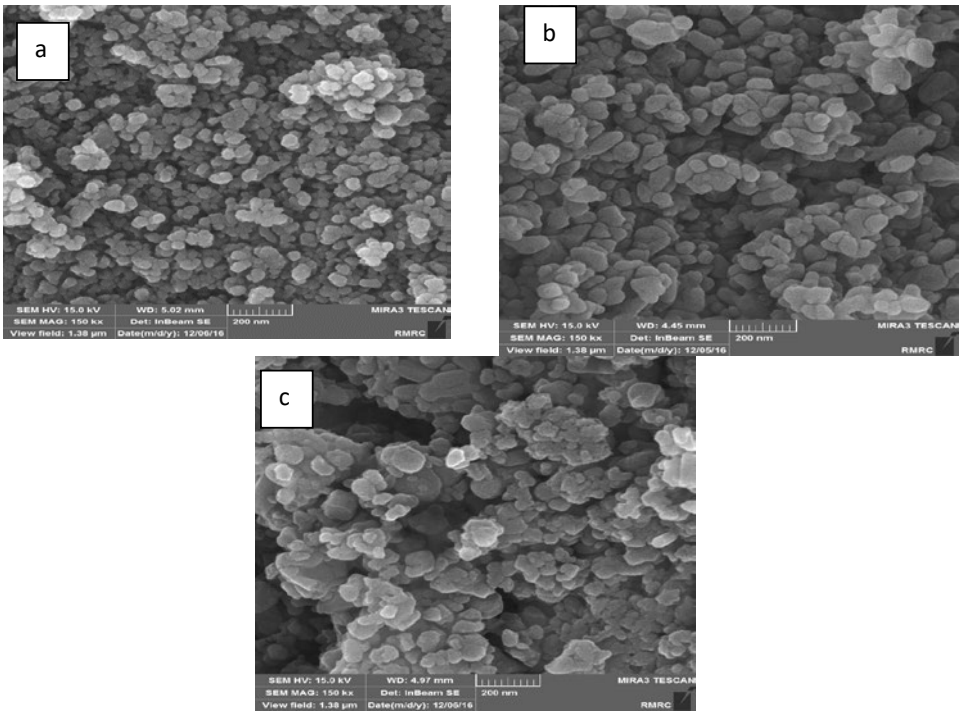

Fig. 15. Field emission SEM images of S53P4 bioglass-fluorapatite nanocomposites a) 10%, b) 20%, c) 30% of S53P4 bioglass

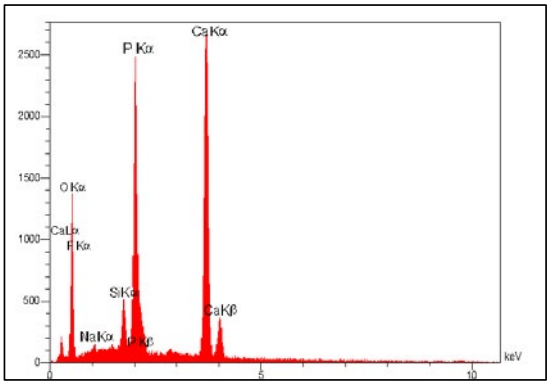

Fig. 16. EDS analysis of BG-FA nanocomposites

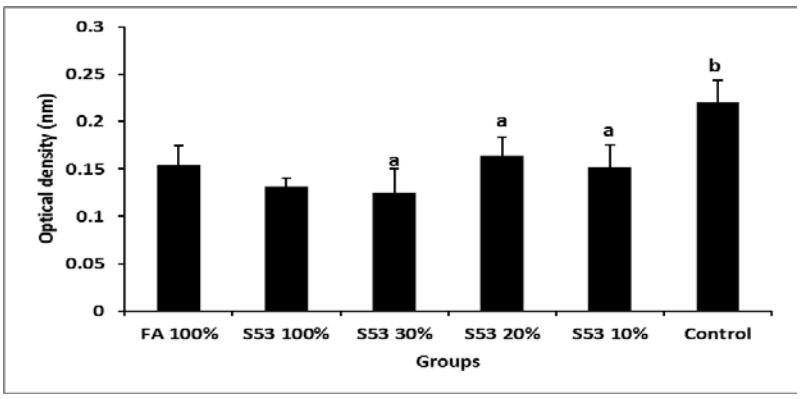

Fig. 17. MTT cell survival test for all samples after 24 h

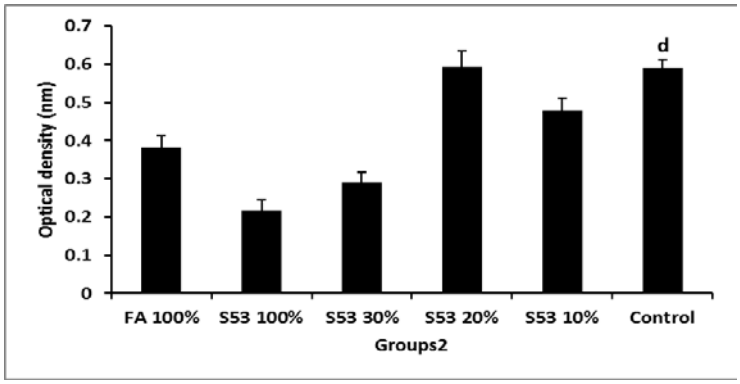

Fig. 18. MTT cell survival test for all materials after 7 days

Table 4. The results of MTT cell survival test for all samples after 24 h

OD 24 h	Mean	Standard Error (SE)
FA 100%	0.154	0.021
S53 100%	0.131	0.009
S53 30%	0.125	0.025
S53 20%	0.164	0.02
S53 10%	0.152	0.024
Control	0.22	0.024

Table 5. The results of MTT cell survival test for all materials after 7 days

OD 7 days	Mean	Standard Error (SE)
FA 100%	0.382	0.031
S53 100%	0.216	0.029
S53 30%	0.292	0.024
S53 20%	0.593	0.041
S53 10%	0.479	0.031
Control	0.59	0.0223

The EDS pattern of the FA-BG nanocomposites that was shown in Fig. 16 expressed the peaks of oxygen, fluorine, silicon, phosphorus and calcium without the effects of other foreign elements, which can be attributed to the high elemental purity of synthesized nanocomposites.

The results of the MTT test (3-(4,5-dimethylthiazol -2-yl)-2,5-diphenyltetrazolium bromide) after 24 h and 7 days are presented in Figs. 17 and 18; and also Tables 4 and 5. It can be observed that by increasing the time of cell placement with the extract in all three main samples, negative control and positive control of cellular responses increased by 10 and 20% of S53P4 bioglass, but with increasing of 30% S53P4 bioglass of cell survival was decreased.

CONCLUSION

S53P4 nanobioactive glass and nano-florapitate has been prepared by modifying sol-gel method and nanobioactive fourapitate nanocomposite with 10%, 20% and 30% S53P4 bioglass has been prepared by modifying sol- gel method at 600 °C with particle size ranging between 20-30 nm. The crystallinity of the nanocomposites, by increasing the percentages of S53P4 nanobioactive glass from 10 to 30% decreased from 86 to 67%, and the average diameter of the crystals were increased from 21nm to 29 nm. The result of MTT assay indicated nontoxicity.

CONFLICT OF INTEREST

The authors declare that there is no conflict of interests regarding the publication of this manuscript.

REFERENCES

[1] A. Seyedmajidi, R. Rajabnia and M. Seyedmajidi, J. Lab. Physicians, 10, 265 (2018).
[2] F. Sayyedan, A. Fathi, M Hossein Edris, A. Doostmohammadi, V. Mortazavi and F. Shirani, Dent. Res. J. (Isfahan), 10, 452 (2013).
[3] C. Soundrapandian, Aaps. Pharmscitech, 11, 1675 (2010).
[4] L. Hench, J. Mater. Sci-Mater. M., 17, 967 (2006).
[5] E. Mancuso, Ceram. Int., 43, 12651 (2017).
[6] M. Kheradmandfard, J. Alloy Compd, 504, 141 (2010).
[7] N. Shankhwar, RSC Adv., 5 100762 (2015).
[8] S. Joughehdoust, A. Behnamghader and A. Afshar, Iranian Journal of Pharmaceutical Sciences Iran. J. Pharm. Sci., 4, 169 (2008).
[9] N. Jmal, J. Bouaziz, Mater. Sci. Eng. C., 71, 279 (2017).
[10] W. Chen, Chem. Geol., 451, 183 (2017).
[11] P. Khoshakhlagh, Carbohydr. Polym., 157, 1261 (2017).
[12] S. Joughehdoust and S. Manafi, Mater. Sci-Poland, 30, 45 (2012).
[13] F. Stabile, Ceram. Int., 42, 4507 (2016).
[14] F. Barandehfard, Ceram. Int. 42, 17866 (2016).
[15] S. Santos, L.S. Barreto and E.A dos Santos, Non-Cryst., Solids, 439, 30 (2016).
[16] J. Shen, Mater. Design, 97, 204 (2016).
[17] S. Joughehdoust, A. Behnamghader, A.H. Rajabi Zamani, In Proceedings of NanoCon, Olomouc, Czech Republic (2010).
[18] S. Sumathi and B. Gopal, J. Cryst. Growth, 422, 36 (2015).
[19] K. Roche and K.T. Stanton, J. Fluorine Chem., 161, 102 (2014).
[20] J. Zhao, Appl. Surf. Sci., 314, 1026 (2014).
[21] V. Stanic, Appl. Surf. Sci., 290, 346 (2014).
[22] C. Tredwin, Dent. Mater., 29, 521 (2013).
[23] S. Joughehdoust, A. Behnamghader, R. Jahandideh and S. Manafi, J. Nanosci. Nanotechnol., 10, 2892 (2010).
[24] L. Cooper, Biomaterials, 27, 926 (2006).
[25] L. Rodrıguez-Lorenzo, J. Hart and K. Gross, Biomaterials, 24, 3777 (2003).
[26] S. Loher, Chemistry of materials, 17(1), 36 (2005).
[27] N. Lindfors, N., Bone, 47(2), 212 (2008).
[28] M. Rahaman, Acta biomaterialia, 7(6), 2355 (2011).
[29] J. Moradian-Oldak, Matrix Biology, 20(5), 293 (2001).
[30] A. Greenwald, The Journal of Bone & Joint Surgery, 83, 98 (2001).
[31] A. Kolk, Journal of Cranio-Maxillofacial Surgery, 40(8), 706 (2012).
[32] P. Giannoudis, H. Dinopoulos, E. Tsiridis, Injury, 36(3), 20 (2005).
[33] M. Chitsazi, Med Oral Patol Oral Cir Bucal, 16(3), 448 (2011).
[35] A. Gosain, P.S.E.F.D. Plastic and reconstructive surgery, 114(2), 590 (2004).